Robotica (2016) volume 34, pp. 2368–2385. © Cambridge University Press 2015
doi:10.1017/S0263574715000016

Stiffness analysis of multibody systems using matrix structural analysis—MSA

G. D. L. Soares Júnior, J. C. M. Carvalho and R. S. Gonçalves*

Federal University of Uberlandia School of Mechanical Engineering Uberlandia, MG, Brazil.
E-mails:gliglijr@hotmail.com, jcmendes@mecanica.ufu.br

(Accepted January 2, 2015. First published online: February 10, 2015)

SUMMARY
This paper deals with the stiffness analysis of multibody systems using the Matrix Structural Analysis—MSA. This methodology allows us to obtain the stiffness matrix of the structure from the stiffness properties of each element. First the MSA method is described and its application is detailed using an L-structure in order to make easy its understanding. Numerical and experimental results obtained for the L-structure and a 6-RSS parallel manipulator, follow to prove the validity of the methodology.

KEYWORDS: Parallel manipulator; Multibody systems; Stiffness analysis; Matrix structural analysis.

1. Introduction

Multibody systems consist of kinematic chains composed of links that can be rigid or flexible, interconnected by joints. These systems are used in numerous applications in areas such as aerospace and automobile engineering, machine tools, mechanisms, deep sea exploration, medicine and robotics.[1–3] A good example of a multibody system that has been widely studied in recent years is the parallel manipulator.[4]

Parallel manipulators typically consist of a moving platform that is connected to a fixed base by several serial and/or closed chains, called limbs. Such systems can possess better stiffness properties and higher payload capacity than serial architectures, as well as high velocity and acceleration during operation. Furthermore, errors in the joints are not cumulative, which contributes to these system's overall accuracy. Due to their characteristics, parallel manipulators have been studied extensively from both the theoretical and practical viewpoints. Prototypes have been conceived and built, hand in hand with the development of theoretical investigations into their kinematics and dynamics. The attention of researchers and developers has focused on a number of possible applications such as manipulation,[5,6] packing and assembly/disassembly machines,[7] motion simulation,[8–11] milling machines,[12] toys and sensors. However, these systems have some open problems such as small and complex workspace with internal singularities, stiffness and complexity of their direct kinematics.[5,13,14]. This paper deals with the study of stiffness analysis of multibody systems.

Stiffness can be defined as the capacity of a mechanical system to bear loads without excessive changes in its geometry.[15–17] These geometrical changes in response to applied loads are known as deformations or compliant displacements.

Compliant displacements in a multibody system produce negative effects on static and fatigue strength, wear resistance, efficiency (friction losses), accuracy, and dynamic stability (vibrations). The growing importance of high accuracy and dynamic performance of such systems has increased the use of high strength materials and lightweight designs, improving and significantly reducing their cross-sections and weight. However, these solutions also increase structural deformations and

* Corresponding author. E-mail: rsgoncalves@mecanica.ufu.br

https://doi.org/10.1017/S0263574715000016 Published online by Cambridge University Press

may result in intense resonance and self-excited vibrations at high speed.[17–20] Therefore, the study of stiffness is crucial for the design of multibody systems to enable the proper choice of materials, component geometry, shape and size, and interaction among the components. Some examples of design procedures based on stiffness analysis can be found in refs. [21]–[26].

Due to of its importance, we direct the stiffness analysis mainly to robotics.

The overall stiffness of a manipulator depends on several factors, including the size and material of its links, its mechanical transmission mechanisms, actuators and controller.[17,27] In general, a highly stiff mechanism requires many large and heavy parts. However, high speed motion requires that these parts be small and light. Moreover, it should be noted that stiffness is strongly affected by both the position and the mechanical parameters of the structure's parts.[28]

The verification of analytical and numerical models of structural stiffness basically consists of measuring compliant displacements in different directions resulting from the application of static loads. The main disadvantage of this method is the need for time-consuming measurements that can be affected by experimental errors. In this case, statistical planning is required to determine the number of compliant displacement measurements in a given position as a function of the static load applied.

There are three main methods to derive the stiffness model of manipulators.[29,30] These methods are based on calculations of the *Jacobian matrix*;[31,32,56,57] on *Finite Element Analysis* (FEA)[33–38,58,59] and on MSA.[29,30,39–45]

One of the first stiffness analyses was conducted by Gosselin,[13] who mapped the stiffness of a parallel kinematic machine onto its actuated joints while its links were assumed to be perfectly rigid. This approach was also applied by El-Khasawneh and Ferreira[46] and Zhang et al.[31] To take link flexibility into account, this initial model was supplemented by the lumped model developed by Zhang.[47] Flexible links are then replaced by rigid beams mounted on revolute joints plus torsional springs located at the existing joints.[27,36,48]

Huang et al.[49] stated that the use of FEA models is reliable, but these models require remeshing, resulting in very tedious and time-consuming routines.[49] However, these models are well adapted to validate analytical models or some experimental results.[33–38,46,58,59] For example, Bouzgarrou et al.[33] used the FEA model to study the static rigidity and natural frequencies of the T3R1 parallel robot.

Methods based on MSA are simple and easy to implement computationally. Clinton et al.[50] used this approach to derive the stiffness matrix of each element of a Stewart platform and then assemble individual elements into a system's stiffness matrix. This approach is also used by Huang et al.[49] to obtain the stiffness model of a machine frame considered as a substructure. The superposition principle is used to obtain the stiffness model of the machine structure as a whole. The approach is applied to the Gough–Stewart platforms due to its constructive characteristics which segments have only axial forces.

In this paper, the MSA method is used for obtaining the stiffness matrix of multibody systems. This method was chosen due to its easy implementation and to enable the stiffness mapping as a function of kinematic model and characteristics of its elements. The multibody stiffness study is essential for building equipment with high accuracy as applied to the manufacture of parts and robotic surgeries. This paper have the following contributions: the step-by-step detailing of the MSA method and presenting experimental results applied to an L-structure and a parallel structure with six-degrees of freedom (dof).

First, this paper presents a methodology to determine the global stiffness matrix of a multibody system, using MSA, and knowing the stiffness matrix of each structural element. The compliant displacement of the end-effector as a function of the external forces acting on the structure is then mapped based on the stiffness matrix, and the kinematic model of the multibody system is created.

After the MSA methodology is described, followed by a step-by-step explanation of a simple structure comprising two segments and a spherical joint, called an L-structure.

Finally, the MSA methodology will be applied to two structures: the L-structure and a 6-RSS parallel structure. The theoretical results obtained with the MSA method are then compared with experimental results.

2. Matrix Structural Analysis

In this paper, the stiffness matrix is determined using the *MSA* method, also known as the *displacement method* or *direct stiffness method* (*DSM*) which has been a precursor of FEA.[51] Structural analysis methods break up complex systems into component parts, discrete structural elements, with simple

https://doi.org/10.1017/S0263574715000016 Published online by Cambridge University Press

elastic and dynamic properties that can be readily expressed in a matrix form. Because multibody systems are made up of segments and joints, this method makes it easy to determine the structure's stiffness matrix. Discrete structures are composed of elements joined to one another by connecting nodes. When such a structure is loaded, each node suffers translations and/or rotations, which depend on the structure's configuration and boundary conditions. For example, in a fixed linkage system, no displacement occurs. The nodal displacement can be determined from a complete analysis of the structure. The matrices representing the beam and joint are considered building blocks, which, when fitted together according to a set of rules derived from the theory of elasticity, provide the static and dynamic properties of the whole structure.[39]

2.1. Stiffness of joint and beam

The stiffness of a joint can be given by:[41,42]

$$k_{\text{joint}} = \begin{bmatrix} k_c & -k_c \\ -k_c & k_c \end{bmatrix}, \tag{1}$$

where $k_c = diag(k_{tx}, k_{ty}, k_{tz}, k_{rx}, k_{ry}, k_{rz})$; k_{tx}, k_{ty}, k_{tz} are the translational stiffnesses and k_{rx}, k_{ry}, k_{rz} the rotational stiffnesses about the x, y and z Cartesian axes.

Considering a straight bar j with a uniform cross section which moments and forces acts on its extremities, where are considered reference frames i and $i + 1$ and then, δ_x, δ_y, δ_z are the linear compliant displacements and ϕ_x, ϕ_y, ϕ_z the angular ones, both on x, y and z direction respectively.

The stiffness matrix of a jth three-dimensional straight bar (beam or segment) with a uniform cross-sectional area can be expressed as Eq. (2).

$$k_j = \begin{bmatrix} k_{bj} & -k_{bj} \\ -k_{bj} & k_{bj} \end{bmatrix}. \tag{2}$$

Using the elastostatic properties of the bar can obtain a 6×6 symmetrical stiffness matrix k_{bj} that relates the applied forces/moments with displacements as[52]

$$k_{bj} = \begin{bmatrix} \frac{A_j E_j}{L_j} & 0 & 0 & 0 & 0 & 0 \\ 0 & \frac{12 E_j I_{zj}}{L_j^3} & 0 & 0 & 0 & \frac{6 E_j I_{zj}}{L_j^2} \\ 0 & 0 & \frac{12 E_j I_{yj}}{L_j^3} & 0 & -\frac{6 E_j I_{yj}}{L_j^2} & 0 \\ 0 & 0 & 0 & \frac{G_j J_j}{L_j} & 0 & 0 \\ 0 & 0 & -\frac{6 E_j I_{yj}}{L_j^2} & 0 & \frac{4 E_j I_{yj}}{L_j} & 0 \\ 0 & \frac{6 E_j I_{zj}}{L_j^2} & 0 & 0 & 0 & \frac{4 E_j I_{zj}}{L_j} \end{bmatrix} \tag{3}$$

In Eq. (3), E_j and G_j are the modulus of elasticity and the shear modulus of element j respectively; L_j is the beam length, I_{yj}, I_{zj} are the moments of areas about the y and z axes, respectively, J_j is the Saint-Venant torsional constant and A_j is the cross-sectional area.

The application of MSA requires writing the stiffness matrices of all the elements in the same reference frame. This reference transformation must be computed for all the elements before the stiffness matrix of the structure is assembled. The transformation matrix, T_j, can be obtained by linear algebra.[52]

Thus, the stiffness matrix of the elements in a common reference frame (elementary stiffness matrix), for segments, k_j^e, and for joints, k_{joint}^e can be expressed as

$$\left[k_j^e\right] = [T_j]\,[k_j]\,[T_j]^T, \tag{4}$$

$$[k_{\text{joint}}^e] = [T_j]\,[k_{\text{joint}}]\,[T_j]^T. \tag{5}$$

After obtaining the stiffness matrix of beams and joints in a common reference frame, the stiffness matrix of a structure can be determined using MSA. Based on how the structure elements are connected

https://doi.org/10.1017/S0263574715000016 Published online by Cambridge University Press

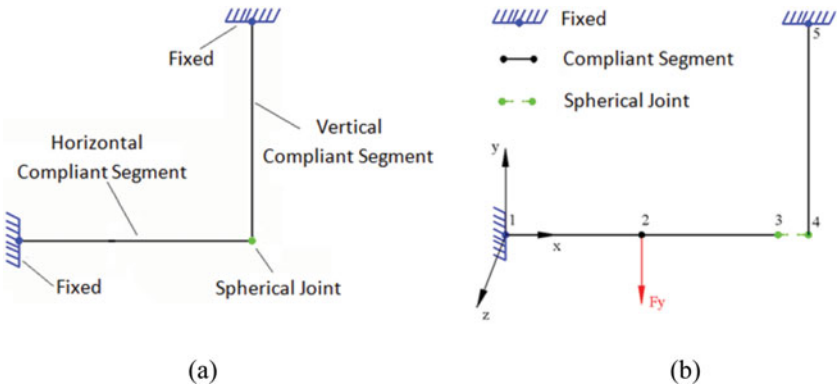


Fig. 1. (a) Scheme of the L model; (b) Nodes of an L-structure.

through their nodes, it is possible to define a connectivity matrix. Since segment and joint stiffness are known, the global stiffness matrix can be obtained by a superposition procedure.

The methodology described to obtain the global stiffness matrix considers the structure as free, i.e., without motion constraints, what makes this matrix be singular. By applying boundary conditions when the displacements are known, a new invertible stiffness matrix K can be obtained, and the compliant displacement can then be computed as

$$\boldsymbol{U} = K^{-1}\,\boldsymbol{W}, \tag{6}$$

where $\boldsymbol{U}$ are the compliant displacements and $\boldsymbol{W}$ are the applied external wrenches.

3. Applying the MSA for Stiffness Analysis of an L-Structure

This example presents a practical method for computer application of the assembly of a structure's stiffness matrix using the MSA method.

The used structure consists of two bars connected by a spherical joint and crimped at the ends, according to the scheme in Fig. 1(a). In order to consider the application of an external force in the horizontal segment a node must be considered at the point of force application. Then, the horizontal segment is split into two parts. The model in Fig. 1(b) is now composed of three segments and one spherical joint: the first segment is defined by nodes 1 and 2, the second segment is defined by nodes 2 and 3 and the third segment by nodes 4 and 5, while the joint is defined by nodes 3 and 4. Nodes 1 and 5 are fixed. It should be noted that the nodes 3 and 4 which define the joints are physically coincident. The L-structure was used because it is quite similar to the arm and forearm of the 6-RSS structure presented in Sections 5 and 6.

Each element (segments and joint) consisting of two nodes has twelve-dof, i.e., six-dof for each node, Fig. 2. The dof are the possible compliant displacements corresponding to linear compliant displacements (δ_{xi}, δ_{yi}, δ_{zi}) and angular compliant displacements (ϕ_{xi}, ϕ_{yi}, ϕ_{zi}), where the sub-index i corresponds to the node's number, Fig. 3.

Each segment and joint has a stiffness matrix written in the local frame, as given by Eqs. (1) and (2), respectively. These matrices have to be written in relation to the inertial frame. According to the node coordinates, this can be done using Eqs. (4) and (5).

The stiffness matrix is assembled by a superposition process, according to the nodes and their dof. For that each dof is assigned an identification number, preferably in increasing sequence, as shown in Table I.

Using the dof numbers, a connectivity matrix can be assembled in which each row represents the dof of each element. Thus, the matrix of connectivity, mat_connect, is given by:

$$\text{mat_connect} = \begin{bmatrix} 1 & 2 & 3 & 4 & 5 & 6 & 7 & 8 & 9 & 10 & 11 & 12 \\ 7 & 8 & 9 & 10 & 11 & 12 & 13 & 14 & 15 & 16 & 17 & 18 \\ 13 & 14 & 15 & 16 & 17 & 18 & 19 & 20 & 21 & 22 & 23 & 24 \\ 19 & 20 & 21 & 22 & 23 & 24 & 25 & 26 & 27 & 28 & 29 & 30 \end{bmatrix} \begin{matrix} \text{segment} & 1-2 \\ \text{segment} & 2-3 \\ \text{joint} & 3-4 \\ \text{segment} & 4-5 \end{matrix} \tag{7}$$

https://doi.org/10.1017/S0263574715000016 Published online by Cambridge University Press

Table I. Node degrees of freedom.

Compliant displacement	Node $i = 1$	Node $i = 2$	Node $i = 3$	Node $i = 4$	Node $i = 5$
δ_{xi}	1	7	13	19	25
δ_{yi}	2	8	14	20	26
δ_{zi}	3	9	15	21	27
ϕ_{xi}	4	10	16	22	28
ϕ_{yi}	5	11	17	23	29
ϕ_{zi}	6	12	18	24	30

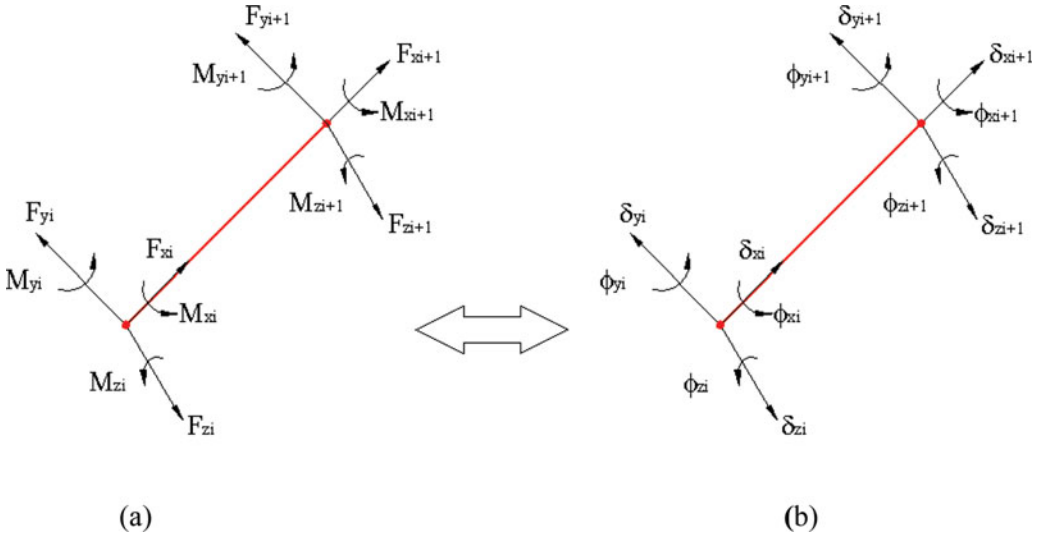


Fig. 2. (a) Representation of forces acting on a bar; (b) corresponding displacements due to deformation of the bar.

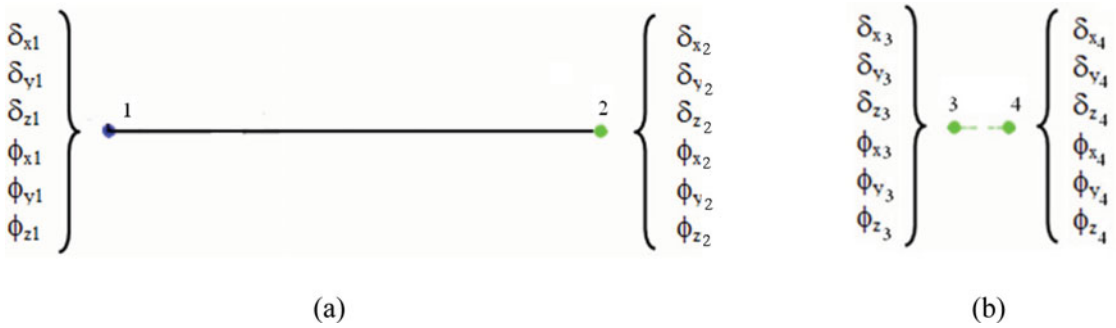


Fig. 3. (a) Segment defined by nodes 1 and 2 with the corresponding compliant displacements; (b) Joint defined by nodes 3 and 4 with the compliant displacements.

The connectivity matrix provides an indication of the elements, its nodes, its dof and which of the elements are superposed.

Therefore, in the assembly of the stiffness matrix, the rows and columns represent the number of dof. As the size of the stiffness matrix is given by the product of the number of nodes multiplied by the number of dof of each node (6-dof), the L-structure has five nodes, then, it has 30-dof. In Fig. 4 each element is represented by a different color, with its corresponding dof. Each position in the matrix has its corresponding element stiffness, and in the overlap region, the sum of the stiffness of the elements that share the same node. Thus, the stiffness matrix of the free structure has a dimension of 30×30, Fig. 4.

Thus, from the connectivity matrix, Eq. (7), it is possible to computationally devise an algorithm to assemble the stiffness matrix.

https://doi.org/10.1017/S0263574715000016 Published online by Cambridge University Press

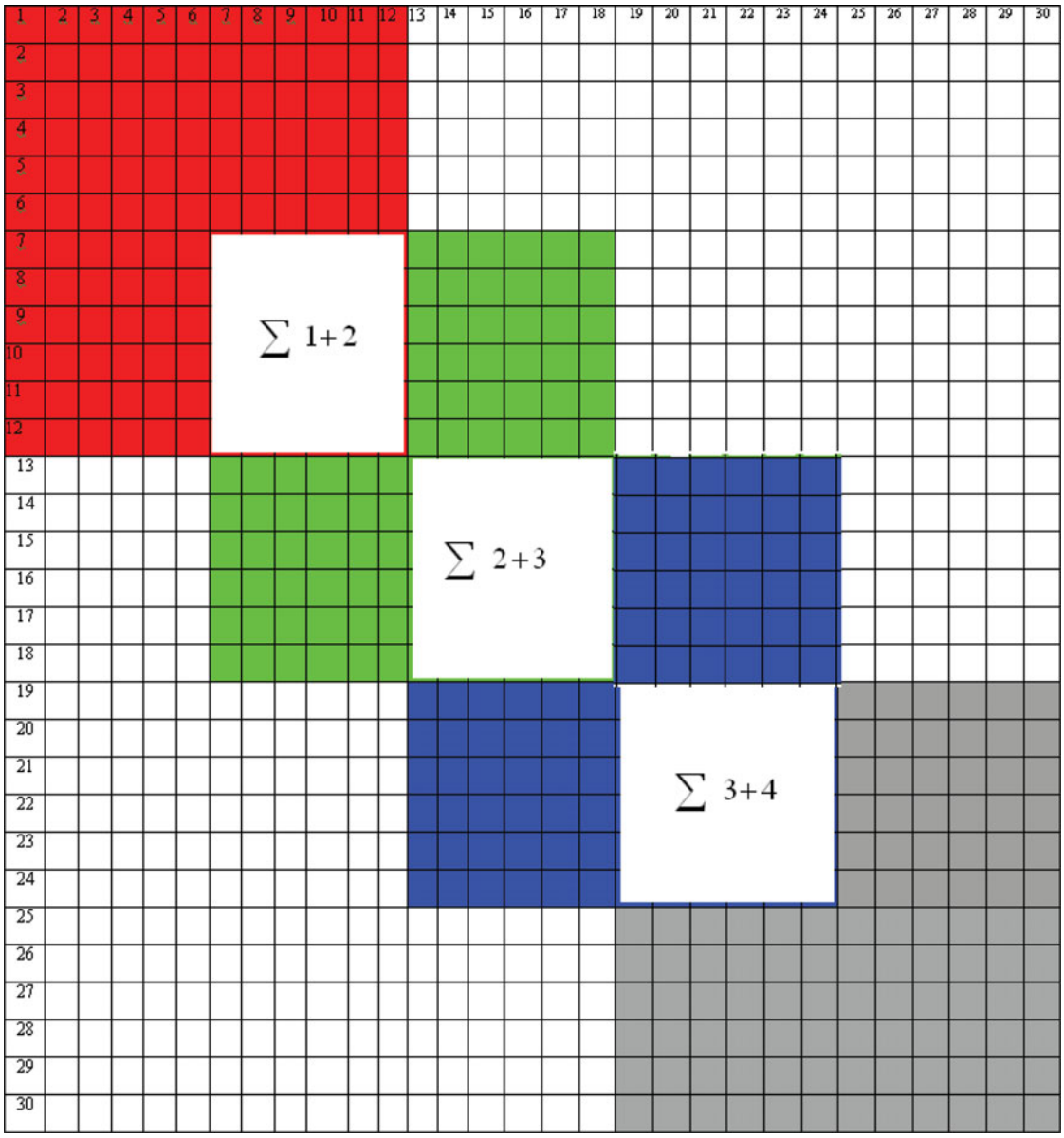


Fig. 4. Superposition procedure to assemble the structure's stiffness matrix.

After obtaining the stiffness matrix of the structure, the boundary conditions must be applied; for this example, they consist of fixed nodes 1 and 5. Because the fixed nodes have zero displacements, the rows and columns corresponding to the dof of nodes 1 and 5 can be deleted, leaving the matrix represented in Fig. 5.

It should be noted that given linear or angular displacements can be imposed as boundary conditions. After the boundary conditions have been imposed, the compliant displacements can be determined as a function of the forces applied at the respective nodes, Eq. (6).

The procedure described in this paper can be extended to any multibody system.

Although the FEA and MSA methods use the same basic equations, Eqs. (2)–(4) and (6), the MSA method can be used as an alternative to the FEA. (a) A robotic structure is composed of segments and joints. Thus, each segment and each joint can be modeled by only two nodes in the MSA method. In contrast, the FEA method involves dividing each beam into several nodes to describe accurately the segment deformed shape, (b) Commercial FEA software programs (the usual procedure) do not allow for control of the solver. In contrast, the MSA method allows the assembly of the stiffness matrix to be followed step-by-step, in the FEA method this procedure is included into an automatic solver. (c)

https://doi.org/10.1017/S0263574715000016 Published online by Cambridge University Press

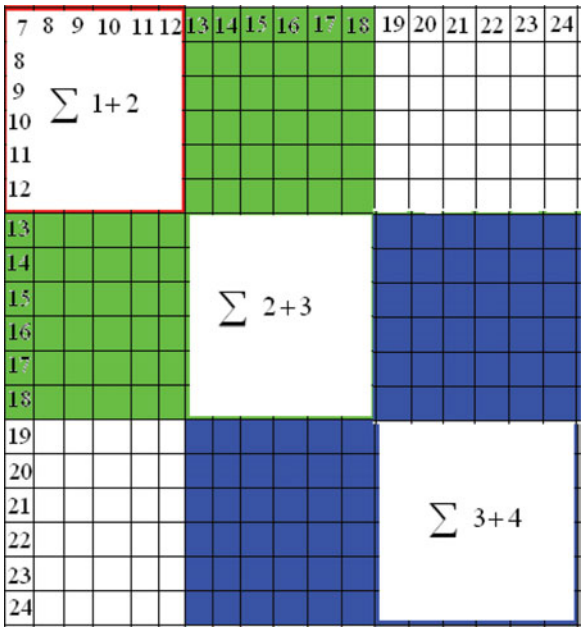


Fig. 5. Final stiffness matrix of the structure.

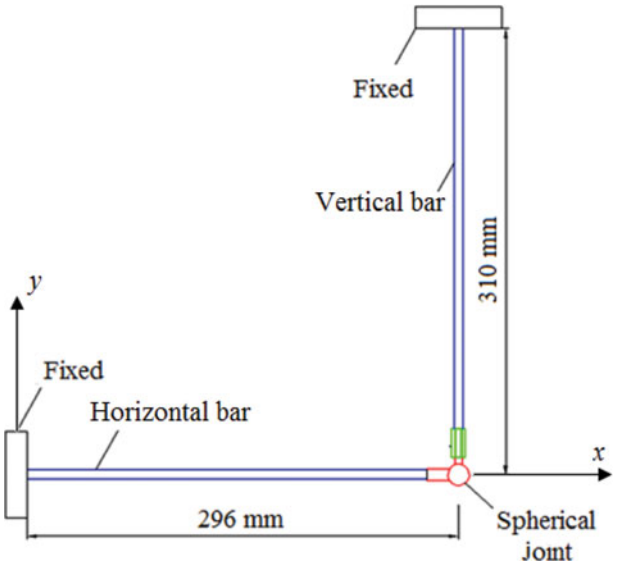


Fig. 6. Scheme of the L-structure.

In the FEA method, each change in the structure's configuration requires remeshing or applying the solver again, thus increasing the computational cost. The MSA method requires only an improvement of the inverse kinematic model to map the stiffness of all the configurations of the structure.

4. Experimental Tests of the L-Structure

The L-structure is composed of two segments connected by a spherical joint and fixed at the other extremities, according to the scheme in Fig. 6.

Figure 7 illustrates the layout of the support structure used in L-structure experiments, which consists of a rigid base. The compliant displacements were measured using a system consisting of a dial indicator with a resolution of 1μm, set in a prismatic precision guide. The dial indicator was positioned along the horizontal segment using a caliper ruler with a resolution of 0.02 mm and a

https://doi.org/10.1017/S0263574715000016 Published online by Cambridge University Press

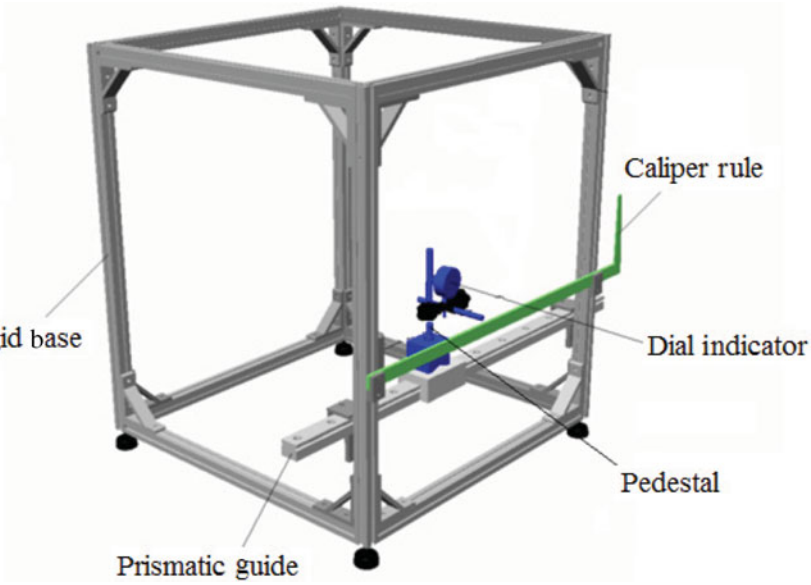


Fig. 7. Schematic diagram of the test bench.

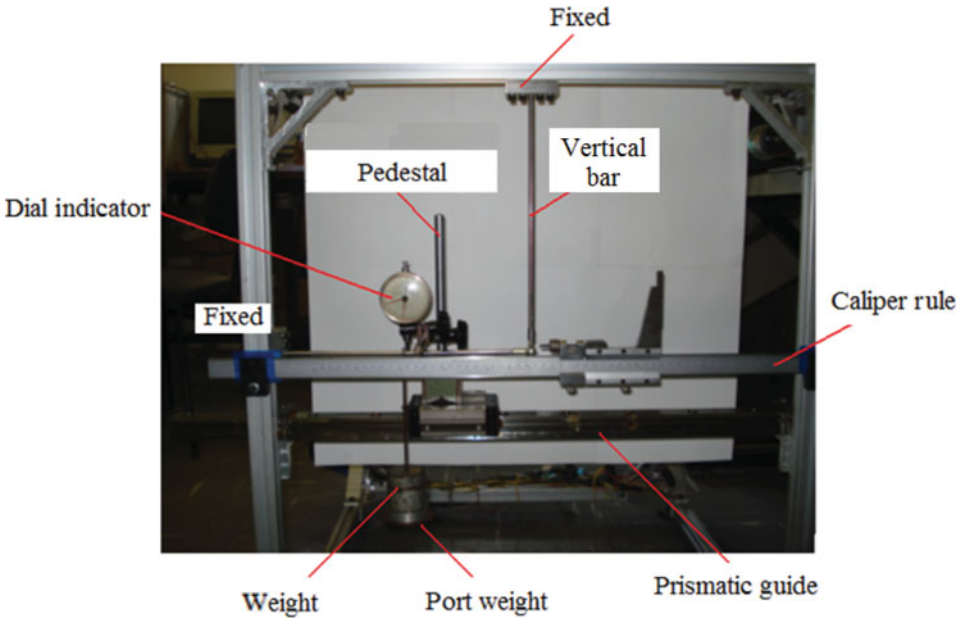


Fig. 8. Details of the experimental apparatus.

course of 600 mm, enabling the position of applied loads to be determined. A digital inclinometer with a resolution of 0.1° was also used for the leveling measurement system, as well as a port weight and weights for the application of static loads, and a digital balance with a resolution of 2 grams to measure the weights, Figs. 7 and 8.

The segments were built of steel with an elastic modulus of $E = 2.17\text{e}^{11}$ N/m^{-2} and circular section with a diameter of 6.1 mm, Fig. 3.

The stiffness of a spherical joint is calculated using $k_c = diag(k_{tx}, k_{ty}, k_{tz}, k_{rx}, k_{ry}, k_{rz})$; while $k_{tx} = k_{ty} = k_{tz} = 2 \times 10^{11}$ are the translational stiffnesses and $k_{rx}, k_{ry}, k_{rz} = 0$ are the rotational stiffnesses.

The experimental stiffness tests of the L-structure were performed with three loads: 0.750 kg, 1002 kg and 1250 kg, measuring the compliant displacement of the y axis along the horizontal segment, Figs. 6 and 8.

https://doi.org/10.1017/S0263574715000016 Published online by Cambridge University Press

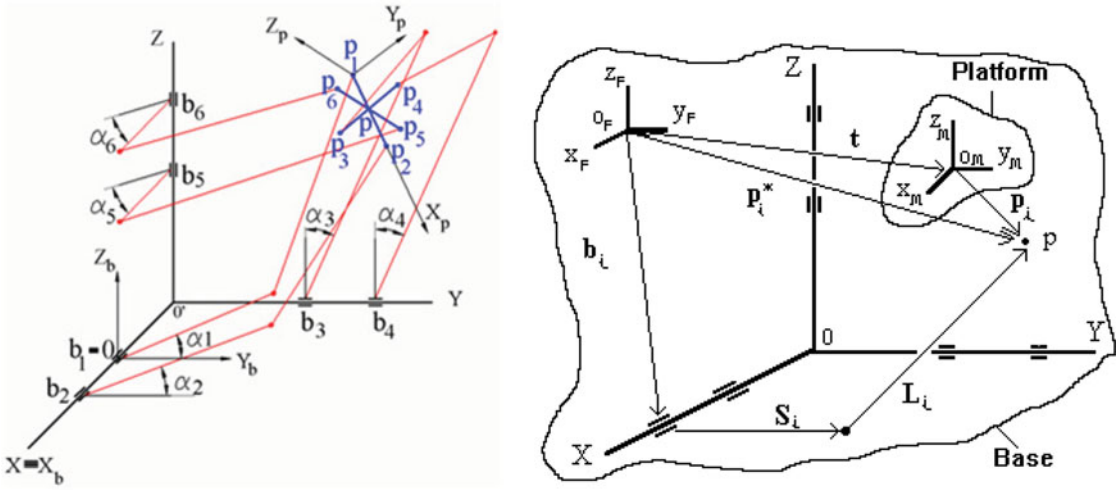


Fig. 9. (a) Generic configuration of a 6-RSS parallel manipulator; (b) Vectors for modeling the 6-RSS structure.

Table II presents the experimental results. A description of the statistical planning is given in.[42–53]

As can be seen in Table II, the differences between the values obtained by MSA and the experimental tests are small. The largest error occurred near the fixed end. This was expected due to the impossibility of obtaining a perfect fixed end and of ensuring that the point where the load was applied was exactly the same point where the displacement was measured.

These results indicate that the MSA method presented in this work is not only easy to understand, implement, and standardize but also provides theoretical results that are consistent with experimental results.

It should also be noted that this example demonstrated the possibility of measuring micrometric compliant displacements.

5. The 6-RSS Parallel Manipulator

The 6-RSS is a parallel manipulator with six-dof, which has a base and a mobile platform connected by six *RS-SS* segments, where the R-joint lies on the Cartesian axes (points b_i), two joints per axis, as shown in Fig. 9(a). The Cartesian system is the base of the structure upon which the actuators are mounted to reduce dead loads. One extremity of S*S*-segments is connected to the mobile platform, which consists of a virtual cube, where the *S*-joints are tied to the center of its faces. The kinematic variables are the input angles α_i ($i = 1$ *to* 6) of the R-joints. The *RS*- and *SS*-segments of this structure have same length $|b_1b_2| = |b_3b_4| = |b_5b_6| = |p_1p_2| = |p_3p_4| = |p_5p_6|$.

Kinematic equations can be obtained by using a suitable analytical procedure with a vector and matrix formulation.[54,55] Equations can be written by considering a generic reference frame fixed to the base ($0_F, x_F, y_F, z_F$) and another to the platform ($0_M, x_M, y_M, z_M$), as illustrated in Fig. 9(b). The parameters are as follows: α_i are the generalized coordinates; $\boldsymbol{b}_i$ is the position vector of the base points b_i (position of the R-joint at the base), $\boldsymbol{S}_i$ and $\boldsymbol{L}_i$ are the vectors of the arm and forearm, all corresponding to the base reference frame, and S_i and L_i are their lengths; $\boldsymbol{p}_i$ is the position vector of the platform points p_i (position of the S-joint of the mobile platform), corresponding to the mobile reference frame. All the parameters are for $i = 1$ *to* 6.

From Fig. 9(b), for $i = 1$ *to* 6, one can obtain:

$$\boldsymbol{L}_i = [R]\,\boldsymbol{p}_i + \boldsymbol{t} - \boldsymbol{b}_i - \boldsymbol{S}_i, \tag{8}$$

https://doi.org/10.1017/S0263574715000016 Published online by Cambridge University Press

https://doi.org/10.1017/S0263574715000016 Published online by Cambridge University Press

Table II. Compliant displacement in the y direction in response to the application of three different loads along the horizontal segment.

Compliant displacement in the y direction [mm]									
	0.750 kg			1,002 kg			1,250 Kg		
x (mm)	δ_y (mm) MSA	Average experimental (mm)	Error (%)	δ_y (mm) MSA	Average experimental (mm)	Error (%)	δ_y (mm) MSA	Average experimental (mm)	Error (%)
30	−0.004	−0.0040	0	−0.005	−0.0060	20	−0.006	−0.0074	23.33
45	−0.011	−0.0102	7.27	−0.014	−0.0152	8.57	−0.017	−0.0182	7.06
60	−0.022	−0.0230	4.55	−0.029	−0.0300	3.45	−0.036	−0.0380	5.56
75	−0.037	−0.0364	1.62	−0.049	−0.0496	1.22	−0.061	−0.0618	1.31
90	−0.054	−0.0536	0.7	−0.072	−0.0710	1.39	−0.090	−0.0926	2.89
105	−0.073	−0.0724	0.82	−0.098	−0.1044	6.53	−0.121	−0.1186	1.98
120	−0.091	−0.0898	1.32	−0.122	−0.1240	1.64	−0.152	−0.1498	1.45
135	−0.107	−0.1114	4.11	−0.143	−0.1406	1.68	−0.179	−0.1764	1.45
150	−0.119	−0.1166	2.02	−0.159	−0.1566	1.51	−0.199	−0.1916	3.72
165	−0.126	−0.1222	3.02	−0.168	−0.1624	3.33	−0.210	−0.2052	2.29
180	−0.126	−0.1204	4.44	−0.169	−0.1636	3.19	−0.211	−0.2038	3.41
195	−0.120	−0.1150	4.17	−0.160	−0.1596	0.25	−0.200	−0.1974	1.30
210	−0.107	−0.1052	1.68	−0.143	−0.1422	0.56	−0.178	−0.1708	4.05
225	−0.088	−0.0836	5	−0.118	−0.1176	0.34	−0.147	−0.1420	3.40
240	−0.066	−0.0640	3.03	−0.088	−0.0812	7.73	−0.110	−0.1074	2.36

where

$$b_{\mathrm{i}} = \left\{ b_{ix} \quad b_{iy} \quad b_{iz} \right\}^t, \tag{9}$$

$$p_{\mathrm{i}} = \left\{ p_{ix} \quad p_{iy} \quad p_{iz} \right\}^t, \tag{10}$$

$$S_{\mathrm{i}} = \left\{ S_{ix} \quad S_{iy} \quad S_{iz} \right\}^t, \tag{11}$$

$$L_{\mathrm{i}} = \left\{ l_{ix} \quad l_{iy} \quad l_{iz} \right\}^t, \tag{12}$$

$$S_i = |\mathrm{S_i}| = \left(S_{ix}^2 + S_{iy}^2 + S_{iz}^2\right)^{1/2}, \tag{13}$$

$$L_i = |\mathrm{L_i}| = \left(l_{ix}^2 + l_{iy}^2 + l_{iz}^2\right)^{1/2}, \tag{14}$$

$$[R] = \begin{bmatrix} \mathrm{n} & \mathrm{o} & \mathrm{a} \end{bmatrix} = \begin{bmatrix} n_x & o_x & a_x \\ n_y & o_y & a_y \\ n_z & o_z & a_z \end{bmatrix}. \tag{15}$$

In Eq. (8), only the lengths L_i of the vector $\boldsymbol{L}_i$ are known. Thus, one can write:

$$\boldsymbol{L}_i^2 = \left([R]\,\boldsymbol{p}_{\mathrm{i}} + t - b_{\mathrm{i}} - S_{\mathrm{i}}\right)^2. \tag{16}$$

Developing Eq. (16), one has:

$$\begin{aligned}
&2p_{ix}\left[\left(n_x t_x + n_y t_y + n_z t_z - n_x S_{ix} - n_y S_{iy} - n_z S_{iz}\right)\right] \\
&+2p_{iy}\left[\left(o_x t_x + o_y t_y + o_z t_z - o_x S_{ix} - o_y S_{iy} - o_z S_{iz}\right)\right] \\
&+2p_{iz}\left[\left(a_x t_x + a_y t_y + a_z t_z - a_x S_{ix} - a_y S_{iy} - a_z S_{iz}\right)\right] + \\
&+2b_{ix}\left[\left(S_{ix} - t_x - n_x p_{ix} - o_x p_{iy} - a_x p_{iz}\right)\right] \\
&+2b_{iy}\left[\left(S_{iy} - t_y - n_y p_{ix} - o_y p_{iy} - a_y p_{iz}\right)\right] \\
&+2b_{iz}\left[\left(S_{iz} - t_z - n_z p_{ix} - o_z p_{iy} - a_z p_{iz}\right)\right] \\
&+\left(t_x^2 + t_y^2 + t_z^2\right) + \mathrm{p}_i^2 + \mathrm{S}_i^2 + \mathrm{b}_i^2 \\
&-2\left(t_x S_{ix} + t_y S_{iy} + t_z S_{iz}\right) - \mathrm{L}_i^2 = 0
\end{aligned} \tag{17}$$

Equation (17) can be simplified by choosing proper reference frames.[55] The reference frames used here are: (X_b, Y_b, Z_b) at the base, where the origin coincides with point b_1; and (X_p, Y_p, Z_p) fixed at the point p_1 of the mobile platform, as illustrated in Fig. 9(a). The rotation matrix $[R]$, Eq. (15), can be given by the Euler angles (rotation ϕ_1 about x, rotation ϕ_2 about y and rotation ϕ_3 about z), where s and c are the abbreviation of sine and cosine, respectively:

$$R = \begin{bmatrix} c\phi_2 c\phi_3 & -c\phi_2 s\phi_3 & s\phi_2 \\ s\phi_1 s\phi_2 c\phi_3 + c\phi_1 s\phi_3 & -s\phi_1 s\phi_2 s\phi_3 + c\phi_1 c\phi_3 & -s\phi_1 c\phi_2 \\ -c\phi_1 s\phi_2 c\phi_3 + s\phi_1 s\phi_3 & c\phi_1 s\phi_2 s\phi_3 + s\phi_1 c\phi_3 & c\phi_1 c\phi_2 \end{bmatrix}. \tag{18}$$

6. Stiffness Analysis of the 6-RSS Parallel Manipulator

In this work, the stiffness model of 6-RSS parallel manipulator using MSA is obtained considering only the compliance of segments. The arms and forearms are modeled as beams, Fig. 10(a), and the stiffness of the entire structure is determined according to the elements arranged in the structure, Fig. 10(b).

The studied structure has the RS-segment and the SS-segment with the same length i.e., $Si = Li = 0.3$ m;$|b_1b_2| = |b_3b_4| = |b_5b_6| = |p_1p_2| = |p_3p_4| = |p_5p_6| = 0.076$ m; the segments are built with

https://doi.org/10.1017/S0263574715000016 Published online by Cambridge University Press

Table III. Compliant displacements of node 4 for $\alpha_1 = \alpha_2 = \alpha_3 = \alpha_4 = \alpha_5 = \alpha_6 = 0^\circ$. Forces are given in (N) and torques in (Nm).

U		δ_x (m)	δ_y (m)	δ_z (m)	ϕ_x (rad)	ϕ_y (rad)	ϕ_z (rad)
$F_e = (10,0,0)$	MSA	0.002168	−0.000532	−0.000532	0.000857	0.001701	−0.005384
$T_e = (0,0,0)$	FEA	0.002173	−0.000534	−0.000534	0.000854	0.001727	−0.005378
$F_e = (0,10,0)$	MSA	−0.000532	0.002168	−0.000532	−0.005384	0.000857	0.001701
$T_e = (0,0,0)$	FEA	−0.000534	0.002173	−0.000534	−0.005378	0.000854	0.001727
$F_e = (0,0,10)$	MSA	−0.000532	−0.000532	0.002168	0.001701	−0.005384	0.000857
$T_e = (0,0,0)$	FEA	−0.000534	−0.000534	0.002173	0.001727	−0.005378	0.000854
$F_e = (10,10,10)$	MSA	0.001103	0.001103	0.001103	−0.002826	−0.002826	−0.002826
$T_e = (0,0,0)$	FEA	0.001105	0.001105	0.001105	−0.002796	−0.002796	−0.002796

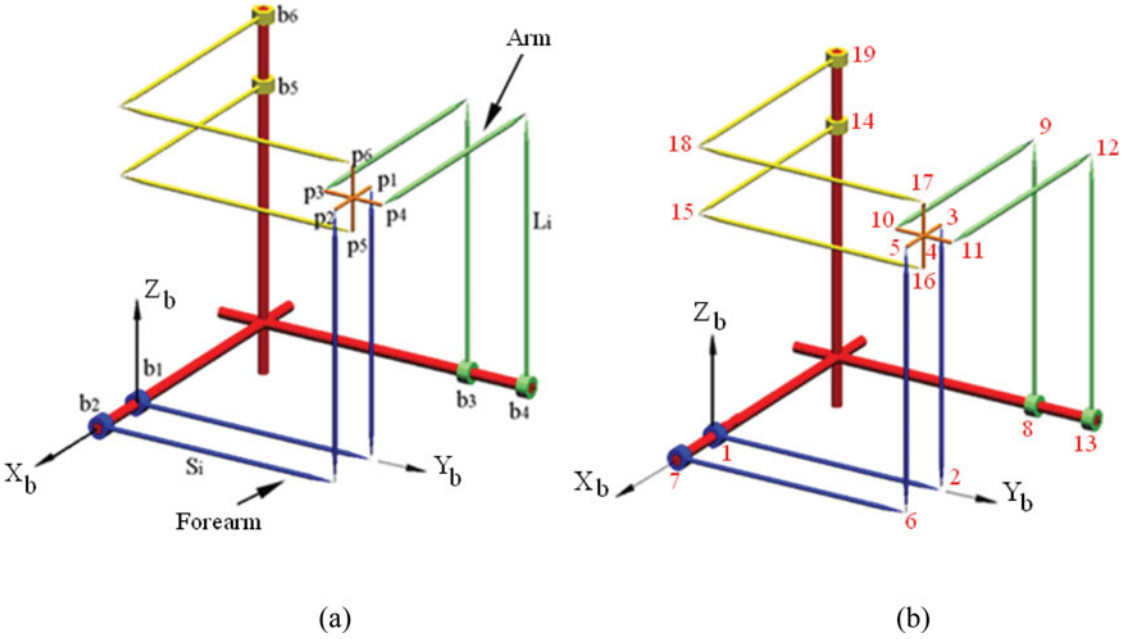


Fig. 10. (a) General arrangement of a 6-RSS parallel manipulator; (b) Nodal points of a 6-RSS parallel manipulator.

steel with $E = 2 \times 10^{11}$ N m^{-2} and $G = 0.8 \times 10^{11}$ N m^{-2}; and the cross-sectional area is circular with *0.005* m diameter. The boundary conditions are given by actuators considered as blocked, and therefore the forearms can be considered fixed in the rotational joints (nodes 1, 7, 8, 13, 14, and 19). The external force and torque are applied on node 4, which is the center of the end-effector.

As can be seen in Fig. 10(b), the structure has 19 nodes with six-dof at each node. Thus, the system has 114-dof with an 18×12 connectivity matrix. The stiffness matrix of the structure, considering the boundary conditions (six fixed rotational joints), is a 78×78 matrix.[42]

To check the analysis made with the MSA method, a model was built using the FEA method with ANSYS® software. The element used here is a beam divided into 10 parts. The running time to solve the FEA and MSA methods are similar. The running time means that for the MSA method is after the kinematics matricial implementation and for the commercial software the structure mesh is done. The main difference is that the MSA method needs only the kinematic model of the structure and, for the commercial software is necessary to build the FEA model of the structure at each desired configuration.

Tables III and IV list the results obtained from the FEA and MSA models. In these tables, F_e is the external force ($F_e = [Fx, Fy, Fz]$) and T_e the external torque ($T_e = [Mx, My, Mz]$).

Numerical simulations were made to demonstrate the soundness of the model due to symmetry of the structure. The results of these simulations are listed in Table III. As can be seen, the compliant displacements are the same in the direction of the applied forces when the other forces and torques

https://doi.org/10.1017/S0263574715000016 Published online by Cambridge University Press

Table IV. Compliant displacements of node 4 for $\alpha_1 = 1.5°$; $\alpha_2 = 5°$; $\alpha_3 = 1.5°$; $\alpha_4 = 3.5°$; $\alpha_5 = 3°$; $\alpha_6 = 1°$. Forces are given in (N) and torques in (Nm).

U		δ_x (m)	δ_y (m)	δ_z (m)	ϕ_x (rad)	ϕ_y (rad)	ϕ_z (rad)
F_e = (10,0,0) T_e = (1,0,0)	MSA	0.002366	−0.001190	−0.000391	0.008324	0.002119	−0.005466
F_e = (0,10,0) T_e = (0,1,0)	MSA	−0.000456	0.002302	−0.001196	−0.005218	0.008197	0.002205
F_e = (0,0,10) T_e = (0,0,1)	MSA	−0.001146	−0.000462	0.002283	0.002089	−0.005136	0.007933
F_e = (10,10,10) T_e = (1,1,1)	MSA	0.000763	0.000650	0.000696	0.005195	0.005179	0.004672

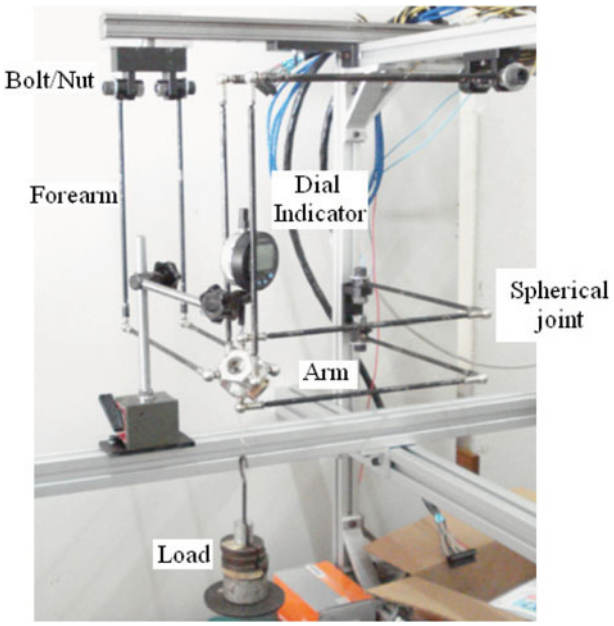


Fig. 11. Experimental stiffness tests of 6-RSS with dial indicator.

are zero, and the compliant displacements are the same when the same forces are applied. Table IV lists the compliant displacements in a generic configuration of the 6-RSS structure.

A non-actuated prototype of the 6-RSS was built for experimental testing, Fig. 11. The actuators, which are blocked with bolts and nuts, are used as boundary conditions (nodes 1, 7, 8, 13, 14 and 19), so the rotational joints can be considered fixed.

The first tests were performed with the initial measurement of compliant displacement in only one direction, using a dial indicator. Three different loads M1 = 0.9935 kg, M2 = 1.2435 kg and M3 = 1.4915 kg were applied on the center of the platform, at node 4. The acceleration of gravity is $g = 9.81$ m s^{-2}. These experimental tests were performed with an initial 6-RSS parallel manipulator configuration of $\alpha_1 = \alpha_2 = \alpha_3 = \alpha_4 = \alpha_5 = \alpha_6 = 0°$.

Compliant displacements in the Z_b direction, at points 3, 5, 11, and 17 were obtained using a dial indicator with a resolution of 1μ m. Statistical planning was used to determine the required number of measurements of compliant displacements, whose results are listed in Table V.

The results listed in Table V confirm the validity of the MSA method, which calculated the compliant displacements in the direction of applied force with an error of less than 9%.

After the experimental tests with the dial indicator, additional measurements were taken with loads applied at points 10 and 16, Fig. 12(b), and different rotations of revolute joints b1 to b4, Fig. 10(a), to determine the compliant displacements in the directions X_b, Y_b and Z_b. The compliant displacements were measured at points 5, 11, and 16 using a Mitutoyo BR-M443 coordinate measuring machine

https://doi.org/10.1017/S0263574715000016 Published online by Cambridge University Press

Table V. Compliant displacements of nodes.

Load	δ_y MSA (mm)	Average experimental (mm)	Standard deviation (mm)	Error (%)
Node 17				
M1	2.136	1.995	0.047	6.6
M2	2.673	2.696	0.047	0.9
M3	3.206	3.201	0.049	0.16
Node 11				
M1	2.250	2.058	0.030	8.5
M2	2.817	2.736	0.028	2.9
M3	3.378	3.460	0.004	2.4
Node 5				
M1	2.062	1.897	0.015	8
M2	2.581	2.540	0.010	1.7
M3	3.096	3.260	0.012	5.3
Node 3				
M1	2.062	2.013	0.004	2.4
M2	2.581	2.731	0.009	5.8
M3	3.438	3.663	0.030	6.5

with a resolution of 0.5μm, Fig. 12(a). Figure 12(c) shows the 6-RSS structure positioned on the BR-M443 measuring machine.

Statistical planning was used to determine the required number of measurements of compliant displacements, whose results are listed in Table VI.

As shown in Table VI, displacements smaller than 1 mm did not yield good results, which can be explained by the clearance in the spherical joints. Another source of error was the inexact point of measurement, which is a point in the center of a spherical joint in the MSA model.

The results listed in Tables V and VI confirm the validity of the MSA method.

7. Conclusions

This paper presented a methodology to obtain stiffness matrices for multibody systems using MSA.

The stiffness matrix enables the compliant displacements of a structure such as a mobile platform to be determined when an external wrench is applied.

The use of this methodology requires knowledge of the kinematic model of the structure and the stiffness matrices of its elements (segments and joints).

To illustrate the use of the MSA method, a simple structure was chosen which is composed by two bars and one spherical joint, called an L-structure. The MSA methodology was applied step-by-step to this structure.

The main advantage of the MSA method to determine the stiffness matrix of a whole structure is that it does not require Jacobian calculations of the structure, and therefore does not require the use of differential equations. Another advantage of this method is that it enables the mapping of compliant displacements for nodes related to different configurations of the structure.

This paper presented practical examples and experimental tests of the use of the MSA method for obtaining compliant displacements.

The MSA methodology was applied in an L-structure and a 6-RSS parallel structure.

The experimental results obtained for the L-structure (composed of two bars and a spherical joint, fixed at the extremities) showed that the differences between the values obtained by the MSA and the experimental tests are negligible. The largest error occurred near the fixed extremity. This was expected because of the impossibility of obtaining a perfectly fixed extremity and of ensuring that the point of applied load was exactly the same point where the displacement was measured.

It should also be noted that the experimental results of the L-structure demonstrated the possibility of measuring small compliant displacements in the order of microns.

To simplify the stiffness model of the 6-RSS parallel structure, only the stiffness of the segments was considered. Blocked actuators were used as boundary conditions, allowing the rotational joints

https://doi.org/10.1017/S0263574715000016 Published online by Cambridge University Press

https://doi.org/10.1017/S0263574715000016 Published online by Cambridge University Press

Table VI. Compliant displacements of nodes.

Applied loads (kg)		Measurements														
			MSA (mm)			Experimental measurements (mm)				Error (%)			Rotating joints (°)			
node 10	node 16	Node	X	Y	Z		X	Y	Z	X	Y	Z	b_1	b_2	b_3	b_4
0	1,641	5	−0,817	3,782	−0,857	Avg. Exp.	−0,684	3,810	−0,701	16,2	−0,7	18,2	0	0	0	0
						Std. dev.	0,180	0,121	0,041							
1,441	0,598	5	−2,854	−0,587	1,064	Avg. Exp.	−2,919	−0,727	1,196	−2,3	−23,7	−12,4	0	0	0	0
						Std. dev.	0,094	0,073	0,119							
1,233	0,700	5	−2,643	−0,551	0,949	Avg. Exp.	−2,545	−0,536	1,618	3,7	2,7	−70,6	5,4	6,6	0	0
						Std. dev.	0,336	0,059	0,275							
1,241	0	11	−2,638	0,892	0,740	Avg. Exp.	−2,602	0,303	0,638	1,4	66,0	13,8	0	0	0	0
						Std. dev.	0,113	0,052	0,065							
1,438	0,601	11	−2,744	−0,280	1,189	Avg. Exp.	−2,790	−0,401	1,322	−1,7	−43,4	−11,1	0	0	0	0
						Std. dev.	0,360	0,054	0,067							
1,233	0	16	−2,262	0,960	0,342	Avg. Exp.	−2,211	0,480	0,607	2,2	50,0	−77,3	2,1	5	−6,1	−4,9
						Std. dev.	0,040	0,111	0,223							
1,233	0	16	−2,366	0,788	0,761	Avg. Exp.	−2,441	0,328	0,365	−3,2	58,4	52,1	2,1	5	2,3	5,7
						Std. dev.	0,036	0,210	0,236							

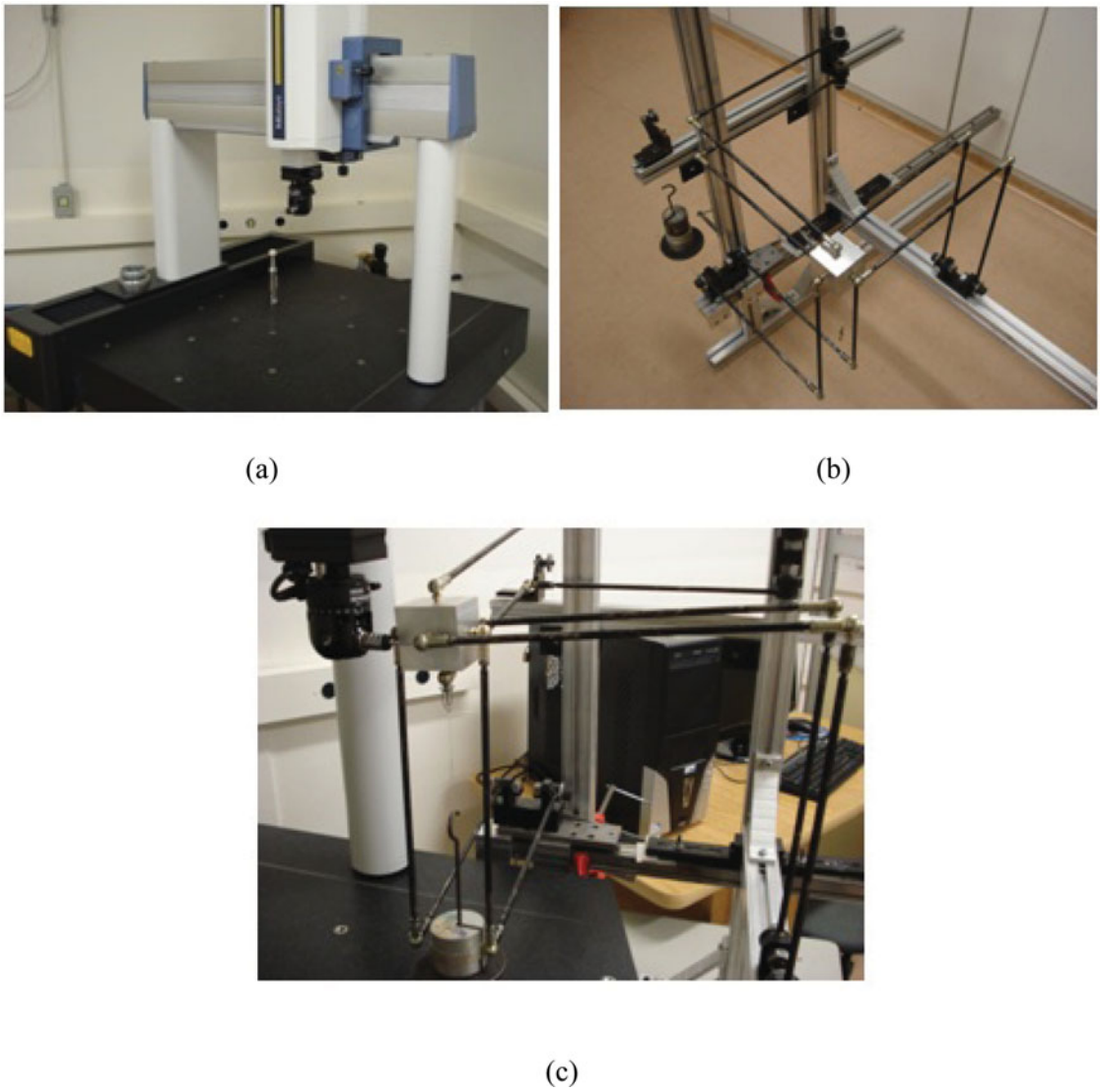


Fig. 12. (a) Mitutoyo BR-M443 coordinate measuring machine; (b) 6-RSS structure; (c) Experimental stiffness tests.

to be considered fixed. To evaluate the method, the numerical results were first compared with a built model and solved using a commercial finite element software program. Experimental tests were then performed in a single direction, the direction of applied load, using a dial indicator. A coordinate measuring machine was used to measure the compliant displacements in three directions.

Based on the results obtained with the L-structure and the 6-RSS parallel structure, it can be stated that the MSA method described in this work is not only easy to understand, implement, and standardize but also provides results that are consistent with experimental test results.

Furthermore, the methodology can be applied to analyze the stiffness of any multibody system.

The next step in this work will consist of improving the stiffness model of the 6-RSS parallel manipulator considering the compliance and clearance of spherical joints.

Acknowledgements

The authors gratefully acknowledge National Council for Scientific and Technological Development (CNPq), Coordination for Improvement of Higher Education Personnel (CAPES) and Foundation for the Support to the Researches in Minas Gerais (FAPEMIG) for their financing of this research work.

https://doi.org/10.1017/S0263574715000016 Published online by Cambridge University Press

References

1. A. D. Dimarogonas, *Machine Design: A CAD Approach* (John Wiley and Sons, Inc. N.Y., 2001).
2. R. S. Hartenberg and J. Denavit, *Kinematic Systhesis of Linkages* (Mc Graw-Hill, New York, 1964).
3. T. G. Chondros, "Archimedes life works and machines," *J. Mech. Mach. Theory* **45**, 1766–1775 (2010).
4. J. P. Merlet, *Parallel Robots*, 2nd ed. (Kluwer, Dordrecht, 2005).
5. E. Macho, O. Altuzarra, C. Pinto and A. Hernandez, "Workspaces associated to assembly modes of the 5R planar parallel manipulator," *Robotica* **26**(3), 395–403 (May 2008).
6. A. Figielski, I. A. Bonev and P. Bigras, "Towards development of a 2-DOF planar parallel robot with optimal workspace use," *2007 IEEE International Conference on Systems, Man, and Cybernetics*, Montréal, QC, Canada, (2007) pp. 7–10.
7. D. Stewart, "A Platform Whit Six Degrees of Freedom," *Proceedings of the Institution of Mechanical Engineers*, (1965) Vol. 180, Pt. 1, n. 15, pp. 371–386.
8. M. Ceccarelli, "A new 3 dof spatial parallel mechanism," *Mech. Mach. Theory* **32**(8), 895–902 (1997).
9. N. E. Nava Rodriguez, G. Carbone and M. Ceccarelli, "CaPaMan2bis as Trunk Module in CALUMA (CAssino Low-Cost hUMAnoid Robot)," *Proceedings of the 2nd IEEE International Conference on Robotics, Automation and Mechatronics RAM 2006*, Bangkok, (2006) pp. 347–352.
10. E. Ottaviano and M. Ceccarelli, "An application of a 3-DOF parallel manipulator for earthquake simulations," *IEEE Trans. Mechatronics* **11**(2), 240–146 (2006).
11. E. E. H. Martines, L. Conghui, G. Carbone, M. Ceccarelli and C. S. L. Cajun, "Experimental and numerical characterization of CaPaMan 2bis operation," *J. Appl. Res. Technol.* **8**(1), 101–119 (2010).
12. T. A. Hess-Coelho, G. F. Batalha, D. T. B. Moraes and M. Boczko, "A Prototype of a Contour Milling Machine Based on a Parallel Kinematic Mechanism," *Proceedings of the 32nd Int. Symposium on Robotics*, Seoul, Korea, (2001).
13. C. M. Gosselin and J. Angeles, "Singularity analysis of closed loop kinematic chains," *IEEE Trans. Robot. Autom.* **6**(3), 281–290 (1990).
14. G. Castelli, E. Ottaviano and M. Ceccarelli, "A fairly general algorithm to evaluate workspace characteristics of serial and parallel manipulators," *Int. J. Mech. Based Design Struct. Mach.* **36**, 14–33 (2008).
15. R. S. Gonçalves, R. R. Santos and J. C. M. Carvalho, "On The Performance of Strategies for the Path Planning of a 5R Symmetrical Parallel Manipulator," *Proceedings of the DINCON 2008, 7th Brazilian Conference on Dynamics, Control and Applications*, Unesp at Presidente Prudente, SP, Brazil, (2008).
16. L.W. Tsai, *Robot Analysis: The Mechanics of Serial and Parallel Manipulators* (John Wiley & Sons, New York, 1999).
17. E. I. Rivin, *Stiffness and Damping in Mechanical Design* (Marcel Dekker Inc., New York, 1999).
18. A. D. Dimarogonas and S. A. Paipetis, *Analytical Methods in Rotor Dynamics* (Appl. Sci. Publishers, London, 1983).
19. A. D. Dimarogonas, *Vibration for Engineers*, 2nd ed. (Prentice-Hall International Editions, Upper Saddle River, New Jersey, 1996).
20. T. G. Chondros and A. D. Dimarogonas, "Identification of cracks in welded joints of complex structures," *J. Sound Vib.* **69**(4), 531–538 (1980).
21. G. Carbone and M. Ceccarelli, "A comparison of indices for stiffness performance evaluation," *Proceedings of the 12th IFToMM World Congress*, Besançon, France (2007) pp. n.A831.
22. X.-J. Liu, Z.-L. Jin and F. Gao, "Optimum design of 3-Dof spherical parallel manipulators with respect to the conditioning and stiffness indices," *Mech. Mach. Theory* **35**(9), 1257–1267 (2000).
23. N. Simaan and M. Shoham, "Stiffness Synthesis of a Variable Geometry Planar Robot," **In:** *8th International Symposium on Advances in Robot Kinematics ARK 2002* (J. Lenarcic and F. Thomas, eds.) (Kluwer Academic Publishers, Caldes de Malavella, 2002) pp. 463–472.
24. G. Carbone, H. O. Lim, A. Takanishi and M. Ceccarelli, "Optimum Design of a New Humanoid Leg by Using Stiffness Analysis," *Proceedings of the 12th International Workshop on Robotics in Alpe-Andria-Danube Region RAAD 2003*, Cassino, (2003), paper 045RAAD03.
25. B. Lim and F. Park, "Minimum vibration mechanism design via convex programming," *J. Mech. Design* **131**(1), 110091–110099 (2009).
26. C. Menon, R. Vertechy, M. Markot and V. Parenti-Castelli, "Geometrical optimization of parallel mechanism based in natural frequency evaluation: Application to a spherical mechanism for future space applications," *IEEE Trans. Robot.* **25**(1), 12–24 (2009).
27. M. Ceccarelli, *Fundamentals of Mechanics of Robotic Manipulation* (Kluwer, Dordrecht, 2004).
28. W. K. Yoon, T. Suehiro, Y. Tsumaki and M. Uchiyama, "Stiffness analysis and design of a compact modified delta parallel mechanism," *Robotica* **22**, 463–475 (2004).
29. D. Deblaise, X. Hernot and P. Maurine, "A Systematic Analytical Method for PKM Stiffness Matrix Calculation," *Proceedings of the IEEE International Conference on Robotics and Automation*, (2006).
30. R. S. Gonçalves and J. C. M. Carvalho, "Stiffness Analysis of Parallel Manipulator Using Matrix Structural Analysis," *Proceedings of the EUCOMES 2008, 2nd European Conference on Mechanism Science*, Cassino, Italy, (2008) pp. 255–262.
31. D. Zhang, F. Xi, C. M. Mechefske and S. Y. T. Lang, "Analysis of parallel kinematic machine with kinetostatic modeling method," *Robot. Comput.-Integr. Manuf.* **20**(2), 151–165 (2004).
32. F. Majou, C. M. Gosselin, P. Wenger and D. Chablat, "Parametric Stiffness Analysis of the Orthoglide," *Proceedings of the 35th International Symposium on Robotics*, Paris, France, (2004).

https://doi.org/10.1017/S0263574715000016 Published online by Cambridge University Press

33. B. C. Bouzgarrou, J. C. Fauroux, G. Gogu and Y. Heerah, "Rigidity Analysis of T3R1 Parallel Robot with Uncoupled Kinematics," *Proceedings of the 35th International Symposium on Robotics*, Paris, France, (2004).
34. C. Corradini, J. C. Fauroux, S. Krut and O. Company, "Evaluation of a 4 Degree of Freedom Parallel Manipulator Stiffness," *Proceedings of the 11th World Cong. in Mechanism & Machine Science, IFTOMM'2004*, Tianjin, China, (2004).
35. J. Enferadi and A. A. Tootoonchi, "Accuracy and stiffness analysis of a 3-RRP spherical parallel manipulator," *Robotica* 1–17 (2010).
36. A. Pashkevich, D. Chablat and P. Wenger, "Stiffness analysis of overconstrained parallel manipulators," *Mech. Mach. Theory*, **44**, 966–982 (2009).
37. B. Li, H. Yu, Z. Deng, X. Yang and H. Hu, "Stiffness modeling of a family of 6-DoF parallel mechanisms with three limbs based on screw theory," *J. Mech. Sci. Technol.* **24**, 373–382 (2010).
38. C. Pinto, J. Corral, A. Oscar and A. Hernández, "A methodology for static stiffness mapping in lower mobility parallel manipulators with decoupled motions," *Robotica*, **28**, 719–735 (2009).
39. J. S. Przemieniecki, *Theory of Matrix Structural Analysis* (Dover Publications, Inc., New York, 1985).
40. W. Dong, Z. Du and L. Sun, "Stiffness Influence Atlases of a Novel Flexure Hinge-Based Parallel Mechanism with Large Workspace," *Proceedings of IEEE ICRA: Int. Conf. On Robotics and Automation*, Barcelona, Spain, (2005).
41. R. S. Gonçalves and J. C. M. Carvalho, "Singularities of Parallel Robots Using Matrix Structural Analysis," *Proceedings of the XIII International Symposium on Dynamic Problems of Mechanics – DINAME, Angra dos Reis*, RJ, Brazil, (2009).
42. R. S. Gonçalves, Estudo de Rigidez de Cadeias Cinemáticas Fechadas *Thesis*, (Uberlândia, Brazil: Universidade Federal de Uberlândia (in Portuguese), 2009. <repositorio.ufu.br/bitstream/123456789/51/1/EstudoRigidezCadeias.pdf>
43. R. S. Gonçalves and J. C. M. Carvalho, "A Multi-Objective Optimization Design for Parallel Structures," *Proceedings of the 20th International Congress of Mechanical Engineering COBEM2009*, Gramado, Brazil, (2009).
44. R. S. Gonçalves, J. C. M. Carvalho, G. Carbone and M. Ceccarelli, "A General Approach for Accuracy Analysis of Parallel Manipulator with Joint Clearance," *Proceedings of the 20th International Congress of Mechanical Engineering COBEM2009*,Gramado, Brazil, (2009).
45. R. S. Gonçalves, J. C. M. Carvalho, G. Carbone and M. Ceccarelli, "Indices for stiffness and singularity evaluation for designing 5R parallel manipulators," *Open Mech. Eng. J.* **4**, (2010).
46. B. S. El-Khasawneh and P. M. Ferreira, "Computation of stiffness and stiffness bounds for parallel link manipulator," *Int. J. Mach. Tools Manuf.* **39**(2), 321–342 (1999).
47. D. Zhang, Kinetostatic Analysis and Optimization of Parallel and Hybrid Architecture for Machines Tolos *Ph.D Thesis* (Laval University Quebec, Canada, 2000).
48. M. Ceccarelli and G. Carbone, "Numerical and Experimental Analysis of the Stiffness Performance of Parallel Manipulators," *Proceedings of the 2nd International Colloquium Collaborative Research Centre 562*, Braunschweig, (2005) pp. 21–35.
49. T. Huang, X. Zhao and D. J. Whitehouse, "Stiffness estimation of a tripod-based parallel kinematic machine," *IEEE Trans. Robot. Autom.* **18**(1), (2002).
50. C. M. Clinton, G. Zhang and A. L. Wavering, "Stiffness Modeling of a Stewart-Platform-Based Milling Machine," *Proceedings of the Trans. of the North America Manufacturing Research Institution of SME*, Vol. XXV, Lincoln, (1997) pp. 335–340.
51. D. L. Logan, *A First Course in the Finite Element Method*, 5 ed. (Cengage Learning, Stamford, CT, 2011).
52. A. A. Shabana, *Dynamics of Multibody Systems* (John Wiley & Sons, New York, 1989).
53. P. M. Berthouex and L. C. Brown, *Statistics for Environmental Engineers* (Lewis Publishers, Boca Raton, FL, 2002) p. 463.
54. C. A. D. Bezerra, Modelagem Geométrica da Estrutura Cartesiana Totalmente Paralela (In Portuguese) *MSc Thesis* (Brazil: Federal University of Uberlândia, 1996).
55. J. C. M. Carvalho, M. A. V. Duarte and C. R. Ribeiro, "Forward and Inverse Kinematic Model of a Parallel Cartesian Structure Using Neural Network," *Proceedings of the Dynamic Problems of Mechanics (IX DINAME)*, (pp. 207–211. 2001)
56. U. Sudhakar and J. Srinvas, "A stiffness index prediction approach for 3-RPR planar parallel linkage," *Int. J. Eng. Res. Tecnol.* **2**(9), 2747–2751 (2013).
57. C. Guohua, W. Bin, W. Nan and Z. Yanwei, "Stiffness, workspace analysis and optimization for 3UPU parallel robot mechanism," *TELKOMNIKA* **11**(9), 5252–5261 (2013).
58. J. Aginaga, I. Zabalza, O. Altuzarra and J. Nájera, "Improving static stiffness of the 6-RUS parallel manipulator using inverse singularities," *Robot. Comput.-Integr. Manuf.* **28**, (2012).
59. A. Rezaei, A. Akbarzadeh and M. Akbarzadeh, "An investigation on stiffness of a 3-PSP spatial parallel mechanism with flexible moving platform using invariant form," *Mech. Mach. Theory* **51**, (2012).

https://doi.org/10.1017/S0263574715000016 Published online by Cambridge University Press